Atmos. Chem. Phys., 12, 11679–11694, 2012
www.atmos-chem-phys.net/12/11679/2012/
doi:10.5194/acp-12-11679-2012
© Author(s) 2012. CC Attribution 3.0 License.

Atmospheric Chemistry and Physics

Temporal evolution of stable water isotopologues in cloud droplets in a hill cap cloud in central Europe (HCCT-2010)

J. K. Spiegel[1], F. Aemisegger[2], M. Scholl[3], F. G. Wienhold[2], J. L. Collett Jr.[4], T. Lee[4], D. van Pinxteren[5], S. Mertes[5], A. Tilgner[5], H. Herrmann[5], R. A. Werner[1], N. Buchmann[1], and W. Eugster[1]

[1]Institute of Agricultural Sciences, ETH Zurich, Zurich, Switzerland
[2]Institute for Atmospheric and Climate Science, ETH Zurich, Zurich, Switzerland
[3]US Geological Survey, Reston, VA, USA
[4]Department of Atmospheric Science, Colorado State University, Fort Collins, Colorado, USA
[5]Leibniz Institute for Tropospheric Research, Leipzig, Germany

Correspondence to: W. Eugster (eugsterw@ethz.ch)

Received: 16 April 2012 – Published in Atmos. Chem. Phys. Discuss.: 14 June 2012
Revised: 8 November 2012 – Accepted: 20 November 2012 – Published: 6 December 2012

Abstract. In this work, we present the first study resolving the temporal evolution of δ^2H and δ^{18}O values in cloud droplets during 13 different cloud events. The cloud events were probed on a 937 m high mountain chain in Germany in the framework of the Hill Cap Cloud Thuringia 2010 campaign (HCCT-2010) in September and October 2010. The δ values of cloud droplets ranged from -77 ‰ to -15 ‰ (δ^2H) and from -12.1 ‰ to -3.9 ‰ (δ^{18}O) over the whole campaign. The cloud water line of the measured δ values was $\delta^2\mathrm{H} = 7.8 \times \delta^{18}\mathrm{O} + 13 \times 10^{-3}$, which is of similar slope, but with higher deuterium excess than other Central European Meteoric Water Lines. Decreasing δ values in the course of the campaign agree with seasonal trends observed in rain in central Europe. The deuterium excess was higher in clouds developing after recent precipitation revealing episodes of regional moisture recycling. The variations in δ values during one cloud event could either result from changes in meteorological conditions during condensation or from variations in the δ values of the water vapor feeding the cloud. To test which of both aspects dominated during the investigated cloud events, we modeled the variation in δ values in cloud water using a closed box model. We could show that the variation in δ values of two cloud events was mainly due to changes in local temperature conditions. For the other eleven cloud events, the variation was most likely caused by changes in the isotopic composition of the advected and entrained vapor. Frontal passages during two of the latter cloud events led to the strongest temporal changes in both δ^2H (≈ 6 ‰ per hour) and δ^{18}O (≈ 0.6 ‰ per hour). Moreover, a detailed trajectory analysis for the two longest cloud events revealed that variations in the entrained vapor were most likely related to rain out or changes in relative humidity and temperature at the moisture source region or both. This study illustrates the sensitivity of stable isotope composition of cloud water to changes in large scale air mass properties and regional recycling of moisture.

1 Introduction

Stable water isotopologues ($^1H_2{}^{18}O$ and $^1H^2H^{16}O$) are naturally available indicators of atmospheric processes involved in water vapor transport and phase changes on different time scales. By measuring stable water isotope ratios of ice cores, information on past climate can be retrieved (e.g. Dansgaard et al., 1993; Petit et al., 1999; Vimeux et al., 2001; Jouzel et al., 2007). On the time scale of days to years, measurements of stable water isotopologues in precipitation and analyzing their spatial and temporal distribution all over the globe improved our understanding of the hydrological cycle (e.g. Rozanski et al., 1993; Gat, 1996, 2000). In ecology, stable water isotopologues have been used to assess soil evaporation, plant transpiration, drought effects on vegetation and water sources for plants (e.g. Dawson, 1998; Yakir and Sternberg, 2000; Farquhar et al., 2007). For these fields of application, a detailed mechanistic understanding of the isotopic signal in atmospheric water vapor and its changes during transport and precipitation formation is essential.

Stable isotopes are suitable tracers of phase transition as the isotopologues $^1H_2{}^{16}O$, $^1H^2H^{16}O$ and $^1H_2{}^{18}O$ differ in physical properties, like equilibrium vapor pressure and diffusivities, which are important during phase change. Due to the lower vapor pressure of heavy isotopologues, $^1H^2H^{16}O$ and $^1H_2{}^{18}O$ preferentially stay in the liquid phase. Under ambient environmental conditions, the equilibrium isotope fractionation effect (which appropriately describes phase change under saturated conditions) of $^1H^2H^{16}O/^1H_2{}^{16}O$ is approximately 8 times larger than for $^1H_2{}^{18}O/^1H_2{}^{16}O$ (Majoube, 1971; Horita and Wesolowski, 1994). For evaporation at relative humidity below 100 %, the evaporating molecules need to pass a saturated transition layer above the water surface. Consequently, the stable water isotope ratios during evaporation under unsaturated conditions result from a combination of an equilibrium isotope fractionation during the transition from water to vapor and a kinetic isotope fractionation during diffusion through the saturated transition layer. As the diffusivity D decreases with increasing mass ($D_{^1H_2{}^{18}O} < D_{^1H^2H^{16}O}$), the water vapor above the saturated transition layer is more depleted in ^{18}O during evaporation at lower relative humidities than it would be for evaporation at 100 % relative humidity if ^2H is kept constant (Cappa et al., 2003).

Measurements of both hydrogen and oxygen isotope ratios are thus powerful tools to assess the atmospheric water cycle. So far, focus has been set on the isotopic variations in precipitation, for example in the framework of the Global Network of Isotopes in Precipitation (GNIP; Craig, 1961; Dansgaard, 1964; Merlivat and Jouzel, 1979; Rozanski et al., 1993; Araguas-Araguas et al., 1996). As the natural abundance of the heavy water isotopologues is small (0.2005 % for $^1H_2{}^{18}O$ and 0.0155 % for $^1H^2H^{16}O$; Risi, 2009), their isotope ratios are commonly expressed using the δ-notation:

$$\delta = \frac{R_{\text{sample}}}{R_{\text{V-SMOW}}} - 1, \quad (1)$$

where R_{sample} is the isotope ratio of the heavy isotope to the lighter isotope in the sample, and $R_{\text{V-SMOW}}$ is the isotope ratio of Vienna Standard Mean Ocean Water, which serves as an international measurement standard for water isotopologues (IAEA, 2009).

The Global Meteoric Water Line (GMWL: $\delta^2H = 8 \times \delta^{18}O + 10 \times 10^{-3}$) is well-established as the average relation between $\delta^{18}O$ and δ^2H in worldwide precipitation (Craig, 1961). The slope of the GMWL arises from equilibrium isotope fractionation, whereas the intercept (also known as deuterium excess $d_{\text{GMWL}} = \delta^2H - 8 \times \delta^{18}O$) results from kinetic isotope fractionation (Craig, 1961). In colder regions (high latitude and/or altitude), as well as at large distances from the coast, the rain was found to be more depleted in heavy isotopologues than in warmer and coastal regions. The water vapor which forms by evaporation at low temperatures is depleted in heavy isotopologues, resulting in rain with a relatively low δ value, referred to as depleted in ^2H and ^{18}O and sometimes as isotopically "light" rain. Inland regions receive air masses with water vapor that is more depleted in heavy isotopologues due to the prior rain out of the air mass, a process that can be modeled using Rayleigh distillation (Gat, 1996). Consequently, the rain in such regions was also found to be more depleted in heavy isotopologues than in warmer and coastal regions. Interpretation of the deuterium excess in rain has been controversial. On the one hand, the deuterium excess in rain is supposed to deliver information on the climatic conditions in the vapor source region. The deuterium excess decreases with increasing relative humidity by 0.43 ‰ $\%^{-1}$ RH and decreases by 0.4 ‰ $^\circ C^{-1}$ with decreasing temperature during evaporation from the ocean (Craig and Gordon, 1965; Merlivat and Jouzel, 1979). Deuterium excess in precipitation also increases due to moisture recycling (e.g. Gat and Matsui, 1991; Henderson-Sellers et al., 2002; Rhodes et al., 2006; Froehlich et al., 2008). On the other hand, below-cloud evaporation of falling rain droplets decreases the deuterium excess in rain and increases the deuterium excess in water vapor (Rank and Papesch, 2005; Froehlich et al., 2008), overwriting the initial signature of the moisture source region. Therefore, addressing the question of atmospheric water vapor transport via stable water isotopologues in precipitation is difficult. However, measuring deuterium excess in cloud droplets could indeed reveal insights into the initial isotopic signature of the moisture source region, because cloud droplets are not affected by additional kinetic isotope fractionation as rain droplets below the cloud.

So far, studies that measured stable water isotope ratios in cloud droplets were conducted in ground touching clouds, which sometimes also had a larger vertical extent (Scholl et al., 2011). A cloud in contact with the ground is called fog from the meteorological point of view and therefore most authors addressed this as isotopologues in fog. As an advected cloud that intercepts with a mountaintop or slope does not change its microphysical behavior, we will use the terms cloud and fog interchangeably for a cloud touching the ground. Isotopologues in fog water have been used in combination with rain to study water fluxes through the ecosystem (first proposed by Ingraham and Matthews, 1988) as well as to assess the hydrological budget (e.g. Schmid et al., 2010a). For this purpose, fog and rain were sampled at monthly intervals (Dawson, 1998; Ingraham and Mark, 2000; Corbin et al., 2005; Scholl et al., 2007; Fischer and Still, 2007; Scholl et al., 2011) or event wise (Feild and Dawson, 1998; Corbin et al., 2005; Cui et al., 2009; Schmid et al., 2010a,b; Scholl et al., 2011). In most studies, fog water was found to be enriched in heavy isotopologues in comparison to rain water. Fog often condensed from local vapor, which was more enriched in heavy water isotopologues, while rain formed in the upper regions of the cloud from water vapor, which was typically more depleted in heavy water isotopologues (Scholl et al., 2011). Cloud water isotopic signatures could be related to the water vapor source (Scholl et al., 2007). Moreover, Spiegel et al. (2012) experimentally confirmed

that fog droplets do not differ in isotopic composition with respect to droplet size. As most of the studies did not resolve the temporal trends during a single cloud event, it remains unclear, whether the isotopic composition of cloud water stays constant over time or is subject to large changes that have not been identified yet. This potentially leads to misinterpretation of cumulative monthly cloud samples.

In this work, we present the first water isotopic data set resolving in time the δ value variation of individual cloud events during the Hill Cap Cloud Thuringia 2010 (HCCT-2010) campaign in Thuringia in September and October 2010. The primary goal of the present study is to deliver the first δ^2H and δ^{18}O values in cloud droplets measured in Europe and to link them to air mass origin, seasonality, as well as measured δ values in monthly precipitation. Second, a classification of the measured events is proposed, in which two possible mechanisms are identified to explain the observed δ values in cloud water: (1) condensation-driven changes in isotopic composition of the cloud droplets, and (2) changes in the isotopic signature of the water vapor feeding the cloud. Third, we assess how stable water isotopologues in cloud water can be used as a tool to contribute to a better understanding of atmospheric water vapor transport.

2 Material and methods

2.1 Measurement site and HCCT-2010 campaign

Cloud data were collected during the HCCT-2010 campaign, a Lagrangian-type cloud experiment conducted close to the summit of Schmücke (50°39′19″ N/10°46′15″ E, 937 m a.s.l., see Fig. 1) between 14th September and 24th October 2010. Schmücke is nearly the highest elevation of a low mountain range in Germany (Thüringer Wald, see Fig. 1), extending 150 km from NW to SE and 35 km from SW to NE. For south-westerly wind directions (the predominant wind direction; 210° to 250°, Herrmann et al., 2005), this orographic barrier exhibits ideal conditions for Lagrangian-type cloud experiments, cooling the arriving air masses adiabatically by lifting and thus creating an orographic cap cloud. Moreover, low frontal clouds also hit this barrier, resulting in foggy conditions at the mountain top station. Independent of where the cloud forms it is continuously "fed" by the water vapor, which is entrained into the cloud due to overflow over the mountain ridge. These air masses are typically aged, originating either from polar or Mediterranean regions (Scherhag, 1948). They are influenced by anthropogenic emissions originating from Western Europe and by biogenic emissions from local sources like the Rhine-Main area and the Thüringer Wald where Norway spruce is the dominant tree species. Two cloud experiments during the FEBUKO project (= Field Investigations of Budget and Conversions of Particle Phase Organics in Tropospheric Cloud Processes) have been carried out on this mountain ridge before in autumn 2001 and 2002 (e.g. Herrmann et al., 2005).

Fig. 1. Location map including the sample collection site Schmücke (red square), the low mountain range Thüringer Wald (green area), Meiningen (red square, where the DWD launches its meteorological soundings), the closest GNIP station Wasserkuppe Rhön (red square) and Heidelberg (where Jacob and Sonntag (1990) collected the water vapor samples). The map is based on "Atlas der Schweiz" (Hurni, 2010).

2.2 Collection and measurement of cloud water samples

Cloud water samples of three droplet size fractions (4 µm to 16 µm, 16 µm to 22 µm and > 22 µm in diameter) were collected using a three-stage Caltech Active Strand Cloudwater Collector (CASCC), similar to the two-size fraction CASCC presented by Demoz et al. (1996). The CASCC was installed on a 20 m tall measurement tower at the site. Cloud collectors of this type have been used previously for cloud water sampling for isotope ratio analysis (Michna et al., 2007; Scholl et al., 2011) and tests revealed that no significant isotope

fractionation occurs during sampling (Spiegel et al., 2012). We collected a total of 41 cloud samples, each consisting of one vial per sampling stage of the CASCC, distributed over 13, non-raining cloud events with temperatures above 0°C such that liquid clouds only were sampled (Table 1). Wind speed during sampling collection varied between 1 and 12 m s^{-1} for all cloud events. The prevailing wind direction at the site was around 200° to 250°. The sampling interval of each cloud sample varied between 1 and 3 h, and each event consisted of n samples (with n between 1 and 8, depending on the duration of the event).

The samples were analyzed for δ^2H and δ^{18}O using isotope ratio mass spectrometry (Gehre et al., 2004) with an uncertainty of 0.3 δ units (δ^2H) and 0.04 δ units (δ^{18}O, peak-jump method) over all measurements. For details on collection and sampling techniques, we refer to Spiegel et al. (2012) and references therein. For the analysis in this work, we use the volume weighted mean values of the three stages from the CASCC. We used the subscript c (= condensed phase) when referring to the collected cloud water and the subscript v to refer to δ values in the vapor phase (see Sect. 2.4 for details on the modeling procedure).

$$\delta_c = \frac{\sum_{i=1}^{3} V_i \times \delta_i}{\sum V_i}, \quad (2)$$

where V_i is the collected volume and δ_i the measured δ value of stage number i (i= 1,2,3). The measurement error is calculated as:

$$\Delta\delta_c = \frac{\sum_{i=1}^{3} V_i \times \Delta\delta_i}{\sum V_i}, \quad (3)$$

where $\Delta\delta_i$ represents the standard error from the three IRMS measurements performed per vial.

2.3 Auxiliary measurements and tools for data interpretation

For the box model (Sect. 2.4) as well as for the data interpretation (Sect. 3), the following additional measurements and tools were employed:

1. Liquid water content measurement: As input for the model presented in Sect. 2.4, we use the liquid water content (LWC) of the cloud, which was measured close to the tower by a PVM-100 (Particulate Volume Monitor, Gerber Scientific, USA) with 1 min resolution. The PVM-100 measures the LWC by means of light scattering. A detailed description of the PVM-100 measurement setup can be found in Gerber (1991) and Arends et al. (1994).

2. Meteorological measurements: The temperature and air pressure measurements needed to initialize the box model (see Sect. 2.4 for details) were obtained from the weather station (Vantage pro, 1 min resolution), which was mounted on the tower at Schmücke.

3. HYSPLIT backwards trajectories: To interpret the isotopic composition of cloud water based on air mass history, 96-h hourly backward trajectories were calculated with the HYSPLIT model (Draxler and Hess, 1997, 1998; Draxler, 2003), initiated 500 m above ground level (= single run). In addition, an ensemble run was performed, consisting of 26 additional runs with 26 starting points differing ± 250 m in vertical and ± one meteorological grid point in horizontal dimension from the starting point of the single run. The horizontal resolution of the HYSPLIT trajectories is 1° which is about 71.5 km at 50°N, and the temporal resolution is 1 h. Archived data from the global data assimilation system (GDAS) have been used for trajectory calculation.

4. Cumulative rain analysis of the single HYSPLIT trajectories: To address how much water rained out of the measured air masses (Sect. 3.2.3), we first summed up the amount of rain that formed along each trajectory as calculated by HYSPLIT ($\mathrm{Rain_{tr}}$). Then we retrieved the cumulative rain ($\mathrm{Rain_{cu}}$) per cloud sample. This is the total amount of rain that the air masses passing during the sampling interval had formed before reaching Schmücke. $\mathrm{Rain_{cu}}$ is calculated by accumulating $\mathrm{Rain_{tr}}$ of the back-trajectories that started during the sampling interval of each cloud sample. E.g., for a cloud sample collected from 12:15–14:15, the cumulative rain is calculated as:

$$\mathrm{Rain_{cu}} = 0.75 \times \mathrm{Rain_{tr}}(13{:}00) + \mathrm{Rain_{tr}}(14{:}00) + 0.25 \times \mathrm{Rain_{tr}}(15{:}00). \quad (4)$$

5. Synoptic weather charts: We used synoptic charts from the German Weather Service (DWD) with a time resolution of 6 h for the air mass classification and identification of frontal passages (for details see Tilgner et al., 2012).

6. Meteorological soundings: Meteorological soundings were launched in Meiningen 30 km South West (for location of the site see Fig. 1) at 00:00 UTC and 12:00 UTC by the German Weather Service (DWD) (Heinold et al., 2005; Tilgner et al., 2012). From these measurements, the dimensionless Froude number was deduced to characterize the overflow over the mountain ridge (Pierrehumbert and Wyman, 1985):

$$F = \sqrt{\frac{g}{\theta}\frac{\mathrm{d}\theta}{\mathrm{d}z}}\frac{h_m}{U}, \quad (5)$$

where g is the gravitational acceleration [m s^{-2}], θ the potential temperature [K], $\frac{\mathrm{d}\theta}{\mathrm{d}z}$ is the vertical gradient of the potential temperature [K m^{-1}], h_m is the barrier height [m], and U mean wind speed [m s^{-1}]. For Froude numbers below 1, an overflow without blocking effects is expected; for $1 \leq F < 1.5$ small blocking

Table 1. Sampling periods for the 13 cloud events probed during the field campaign HCCT-2010. Additionally, symbols used for the graphs within this study, predominant air mass (according to Scherhag (1948) as classified by Tilgner et al. (2012)), and temperature range during the cloud events are given.

Event	Beginning	End	Symbol	Predominant air mass	Temperature range [°C]
1	14 Sep 11:00	15 Sep 02:00	□	Maritime Air from Northern Atlantic (mTp) Greenlandic polar air (mP)	7.3–10.2
2	24 Sep 23:45	25 Sep 01:45	▷	Warmed Polar air (mPt)	7.8–8.5
3	27 Sep 01:00	27 Sep 07:00	✳	Continental Polar air (cP)	3.9–4.2
4	28 Sep 11:00	28 Sep 13:00	·	North Siberian Polar air (cPa)	6.2–6.6
5	1 Oct 12:00	1 Oct 15:00	◁	Greenlandic Polar air (mP)	6.7–7.2
6	1 Oct 22:30	2 Oct 05:30	△	Greenlandic Polar air (mP)	6–6.3
7[a]	2 Oct 14:30	2 Oct 19:30	◇	Greenlandic Polar air (mP)	6.8–8.1
8	5 Oct 11:00	5 Oct 13:00	+	Mediterranean Tropical air (mTs)	7.8–9.2
9	5 Oct 19:15	6 Oct 06:15	▽	Mediterranean Tropical air (mTs)	9.5–10.6
10	6 Oct 12:15	7 Oct 03:15	◯	Mediterranean Tropical air (mTs)	7.4–10.4
11	19 Oct 21:30	20 Oct 03:30	×	Greenlandic Polar air (mP)	0.4–1.4
12[b]	24 Oct 01:30	24 Oct 08:30	☆	Greenlandic Polar air (mP)	1.7–3.1
13	24 Oct 09:15	24 Oct 11:45	✡	Artic Polar air (mPa)	0.4–1.7

[a] warm front passage
[b] right after cold front passage

effects are expected (= deceleration); for $1.5 \leq F < 2$ blocking effects are expected (= stagnant flow); and for Froude numbers >2 no overflow is expected (= stagnant area upwind of the mountain; Pierrehumbert and Wyman, 1985).

7. Moisture source diagnostic: For the two longest cloud events lasting for 15 h, a detailed moisture source diagnostic was performed as described in Sodemann et al. (2008) and applied in Pfahl and Wernli (2008). Hourly wind analysis data of the regional model COSMO (Steppeler et al., 2003) with a horizontal resolution of 7 km were used to compute kinematic three-dimensional backward trajectories (Wernli and Davies, 1997). Five horizontal starting points were selected in a cross arrangement with the location of the Schmücke hilltop in the center of the cross. The four points defining the cross edges were shifted by 0.2 degree in every direction from the Schmücke hilltop. Nineteen vertical levels were selected as starting points for the trajectories. In the lowest part of the troposphere, trajectories started at every model level (1 to 10), higher up only every second level (10 to 20) and every fifth level (20 to 40). In total, 96 trajectories were computed five days backward in time every hour during the selected events. Several meteorological variables, including specific humidity, 2 m temperature, 2 m dew point temperature, skin temperature and boundary layer height, were interpolated along the backward trajectories. Moisture uptake locations were identified by changes in specific humidity along the trajectories. Only increases in specific humidity in the boundary layer were identified as uptakes. To account for the uncertainty in the boundary layer height parametrization, as well as for the fact that most uptakes of humidity occur at the edge of the boundary layer and the free atmosphere, the boundary layer height was scaled by a factor 1.5 as in Sodemann et al. (2008). Each uptake location was weighted according to its contribution to the final humidity of the trajectory. The assignment of the weights to each uptake was done in a mass consistent way. If a decrease in specific humidity (i.e. rain out) occurred after an uptake, the weights of the previous uptakes were discounted. The final contribution of each trajectory was weighted by its final specific humidity. The meteorological conditions at the uptake points were averaged over the uptake region using the weights determined from the specific humidity contribution.

2.4 Model description

When an air parcel is cooled below its dew point (T_d), cloud droplets form by condensation on preexisting cloud condensation nuclei. With both phases (condensate and vapor) abundant, the isotope ratios of the condensate R_c and the vapor phase R_v are described by the equilibrium isotope fractionation coefficient α as condensation can be considered as an equilibrium isotope fractionation from the isotopic point of view:

$$\alpha(T) = \frac{R_c}{R_v}. \quad (6)$$

Assuming that the cloud droplets are in immediate isotopic equilibrium with the surrounding vapor (Spiegel et al., 2012),

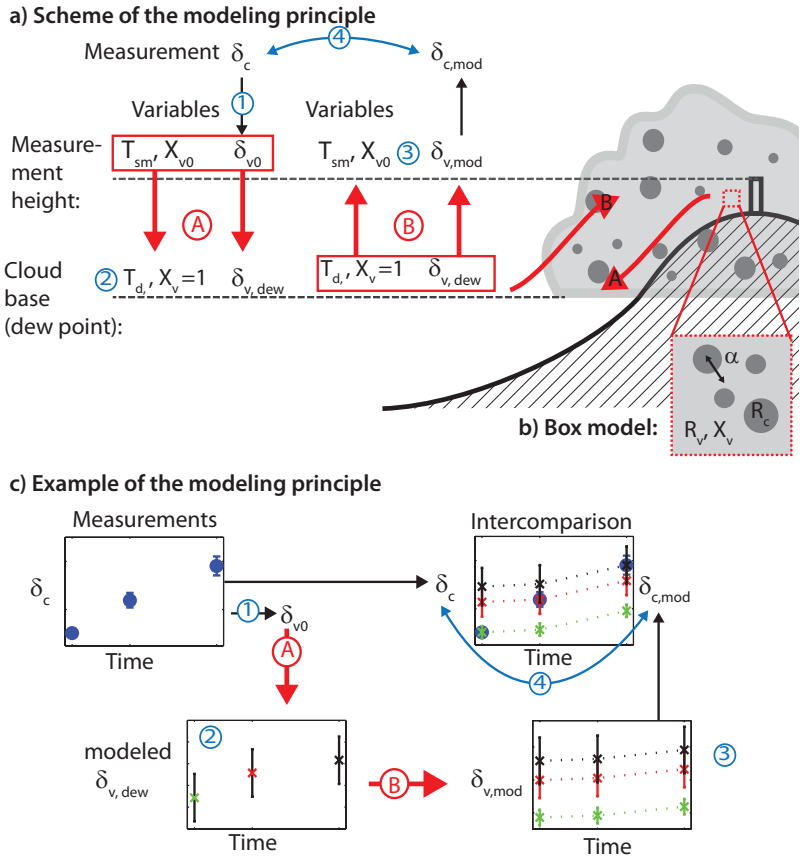

Fig. 2. (a) Sketch of a cloud forming at Schmücke including the box model approach **(b)** consisting of the two model runs A and B. The initial values of each model run are framed in red. **(c)** An example of the modeling principle as described in Sect. 2.4 (variables are explained there as well): from the measured δ_c (blue dots), δ_{v0} is derived ① leading to $\delta_{v,dew}$ after model run A ②. Starting with each of the $\delta_{v,dew}$, model run B produces a series (three in total for the case shown here) of locally thermodynamically driven $\delta_{v,mod}$ ③, from which $\delta_{c,mod}$ were deduced and in a last step compared to the measured time series of δ_c ④. In this example, the transition between the last two measurement points meet the local condensation criterion, because both measured values δ_c are within the errors of modeled values $\delta_{c,mod}$ (cloud sample 2 is within the black error bar, which shows the uncertainty of the $\delta_{c,mod}$ based on $\delta_{v,dew}$ of cloud sample 3 and wise versa). In contrast, the error bar of $\delta_{c,mod}$ based on $\delta_{v,dew}$ of cloud sample 1 (green) does not overlap with cloud sample 2 (and the red error bar not with cloud sample 1). So, the transition from the first to the second measurement point is found to be caused by changes in the water vapor isotope composition feeding the cloud.

the change in the isotope ratio of the vapor phase in response to phase change and to changes in the surrounding conditions (such as temperature) can be modeled for an air parcel (=box) using the following equation (Gedzelman, 1988):

$$\frac{\mathrm{d}R_\mathrm{v}}{R_\mathrm{v}} = \frac{A\,(X_\mathrm{v}-1)\,\mathrm{d}\alpha + (\alpha-1)\,\mathrm{d}X_\mathrm{v}}{X_\mathrm{v} + \alpha A - \alpha A X_\mathrm{v}}. \quad (7)$$

Equation (7) applies to ^{2}H and ^{18}O separately. X_v is the mole fraction of the vapor phase (moles in the vapor phase divided by the moles of condensed and vapor phase). A is the fraction of the condensate remaining in the volume of interest (later on referred to as "box", see Fig. 2b for illustration). Two limiting cases of Eq. (7) are defined by A.

For $A = 1$, the box model is considered to be closed. This means that the condensate formed completely remains in the box and is in thermodynamic and isotopic equilibrium with the surrounding water vapor. In this case, changes in the isotopic composition of vapor and condensate depend on temperature ($\alpha = \alpha(T)$) and liquid water content (as $X_\mathrm{v}(T$, LWC) also depends on LWC). Closed system cloud models have been suggested as an adequate description of a non-raining cloud (Jouzel, 1986) and used for studies on the formation of hail (Facy et al., 1963; Knight et al., 1981).

By setting $A = 0$, the model represents an open system (also known as Rayleigh condensation) where all the condensate (precipitation) is removed immediately. The Rayleigh distillation equation has been used to model the progressive depletion in heavy water isotopologues in precipitation along an air mass trajectory (e.g. Dansgaard, 1964). Moreover, Jouzel (1979) showed that the difference in R_v between the two limiting cases is negligible as long as X_v remains above 0.9.

To evaluate the extent to which condensation controls the variation of measured δ values for the cloud samples, we first used the model (= model run A, in Fig. 2a and c) to obtain the δ value of the water vapor at the dew point ($\delta_{v,dew}$). We then simulated the condensation process by running the model from the dew point to the actual temperature (= model run B, in Fig. 2a and c) and calculated the isotopic signature of the cloud droplets ($\delta_{c,mod}$) based on a certain isotopic signature of the water vapor at the dew point. In a last step, we compared the modeled to the measured δ values at the actual temperature. Because we basically sampled non-raining clouds and because R_v was above 0.94 for all cloud events we used the box model in the closed version for all model runs. Details are given in the next sections.

2.4.1 Model run A: from measured temperature T_{sm} to dew point temperature T_d

First, the box model was first initialized with the measurements. To this end, for every sampling interval we calculated the mean values for the temperature T_{sm}, the liquid water content (LWC) and the dew point (T_d) of the Schmücke cloud from the measured data (see Sect. 2.3). The dew point was calculated from the local mixing ratio w, which itself was determined from the local temperature, air pressure and LWC. In addition to T_{sm} at Schmücke, X_{v0} and δ_{v0} (corresponding to R_{v0}) are needed as initial values (framed in red in Fig. 2). X_{v0} was calculated based on the equilibrium water vapor pressure (vapor phase) and the LWC (condensed phase). R_{v0} – which is the vapor isotope ratio inside the cloud in equilibrium with the condensate – was calculated from measured δ_c values using Eqs. (6) and (1) (Fig. 2 ①)). Herein $\alpha_0 = \alpha(T_{sm})$ was calculated using the equations of Criss (1999, p.103). Second, we repeatedly ran the model for every cloud sample starting with the corresponding T_{sm} down to the dew point T_d, thereby decreasing iteratively T from T_{sm} to T_d and increasing X_v from X_{v0} to 1. This model run is referred to as model run A. By doing so, we calculated the δ_v value for each measurement point for the instant when condensation started (Fig. 2 ②)). We refer to these values as $\delta_{v,dew}$.

2.4.2 Model run B: from dew point temperature T_d to measured temperature T_{sm}

For run B, we used the model a second time in the reversed direction, starting at the dew point T_d and increasing T iteratively to the actually measured temperature T_{sm}. The initial conditions for model run B are T_d, $X_v = 1$ and $\delta_{v,dew}$ as obtained from model run A. For every cloud event we performed n (= number of samples per event) different model runs B, each starting from a different $\delta_{v,dew}$ as obtained from model run A (Fig. 2 ③)). This yielded n^2 calculated δ values (= $\delta_{c,mod}$).

2.4.3 Condensation criteria

In order to evaluate the effect of condensation on the δ_c values, the modeled $\delta_{c,mod}$ values were compared to measured δ_c (Fig. 2 ④)). We categorized the temporal evolution of the measured δ_c value as condensation-driven if the following criteria were fulfilled:

1. The modeled and the measured values were equal within the measurement error ($\delta_c \in [\delta_{c,mod} \pm \Delta\delta_{c,mod}]$ with $\Delta\delta_{c,mod} = 2 \times \Delta\delta_c$).
2. Criteria 1 was fulfilled for two consecutive measurements.
3. Criteria 2 was fulfilled for both δ^2H and δ^{18}O.

3 Results and discussion

For the discussion of the collected data we start from a general and campaign-based context (Sect. 3.1), and then zoom in from the campaign scale to the event scale by focusing on the temporal evolution of individual cloud events (Sect. 3.2).

3.1 Isotopic composition of cloud droplets during HCCT-2010: a campaign-based interpretation

In this section, we describe the measured isotopic signal of the cloud samples in general and compare it to δ values found in precipitation and other fog measurements (Sect. 3.1.1). In Sect. 3.1.2, we discuss the deuterium excess and its link to moisture recycling.

3.1.1 Classification of the observations into the framework of isotopic measurements in precipitation and comparison to other fog measurements

The δ_c values varied from $-77\,‰$ to $-15\,‰$ (δ_c^2H) and from $-12.1\,‰$ to $-3.9\,‰$ (δ_c^{18}O, Fig. 3), during the whole campaign. More detailed information can be found in the raw data set (http://doi.pangaea.de/10.1594/PANGAEA.788629). The temperature range was 0.4 to 10.6°C at Schmücke (Table 1). Highest δ_c values were measured at the beginning of the campaign (14 September), and the lowest δ_c values were measured at the end of the campaign (24 October). Differences in monthly mean values are of the same order as observed in rain and in water vapor in this region (Jacob and Sonntag, 1991, see Table 2). Both the δ values in rain as well as the ones measured in vapor show a clear seasonal pattern with higher values in summer and lower ones in winter. Although the samples of this study were collected only during 6 weeks, the δ trend in the collected samples points towards such a seasonal signal, because monthly differences in δ values agree with the ones from data sets collected over the entire year (Table 2). Interestingly, δ_c values

Table 2. Volume weighted monthly mean values for September and October for the collected cloud water samples at Schmücke (first part). Second part: Differences between the volume weighted mean values for September and October (δ(September) minus δ(October)) for the Schmücke cloud samples. For comparison differences between volume weighted monthly mean values in precipitation for the closest GNIP station (Wasserkuppe Rhön 50°30′ N/9°57′ E, 921 m a.s.l.; 60 km west of the measurement station) as well as for the water vapor values collected in Heidelberg by Jacob and Sonntag (1991) are also given. See Fig. 1 for details on the sites.

Site	Month	Year	δ^{18}O	δ^{2}H
Schmücke	Sep	2010	-5.8 ± 2.5 ‰	-32 ± 21 ‰
Schmücke	Oct	2010	-7.9 ± 1.2 ‰	-48 ± 8 ‰
Schmücke	Sep–Oct	2010	2.1 ‰	17 ‰
Wasserkuppe	Sep–Oct	1978–2007	1.5 ‰	12 ‰
Heidelberg	Sep–Oct	1981–1988	2.4 ‰	18 ‰

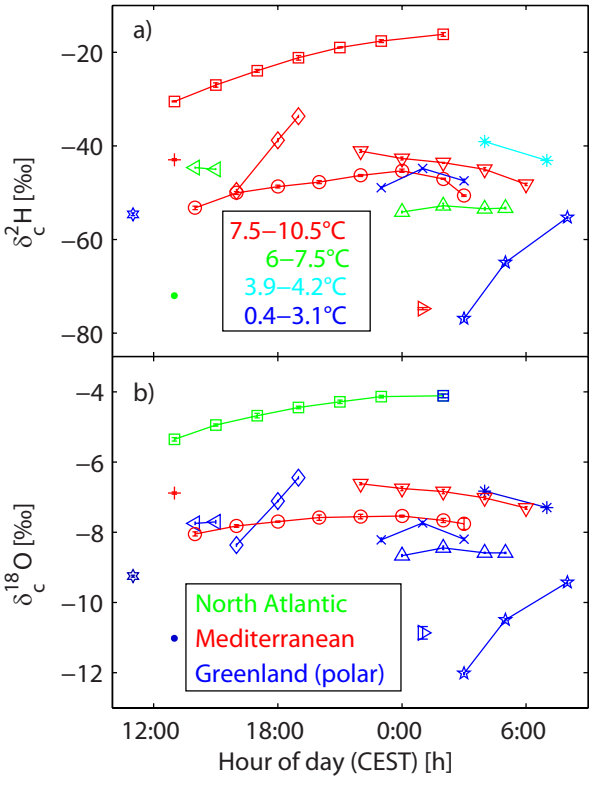

Fig. 3. Diurnal evolution (shown from 10:00 am to 10:00 am next day) of the δ_c^2H and δ_c^{18}O values (including measurement uncertainty Eq. 3) for all measured cloud events during HCCT-2010: The different cloud events are represented with different symbols as summarized in Table 1. Different colors represent **(a)** the temperature range and **(b)** the predominant air mass during the cloud event as classified by Tilgner et al. (2012).

sometimes differed significantly for cloud events with similar local temperature (Fig. 3a and Table 1). As droplets in a hill capture cloud are uniformly in equilibrium with local conditions (Spiegel et al., 2012), differences among cloud events with similar temperatures are strong evidence for differing isotope signatures of the water vapor feeding the cloud.

On the other hand, the air mass origin was only a poor indicator of the δ_c values because cloud water collected during the same week did not differ significantly for different air mass origins (Fig. 3b). The air mass origin is strongly connected to potential rain out processes. The longer the traveling distance of an air mass, the higher the probability that its moisture has been affected by Rayleigh distillation rain out processes. So we could only expect differences in isotopic composition if the traveling distance differed sufficiently for different air mass sources. This was for example the case in the study presented by Rank and Papesch (2005). Due to the very central European measurement location, traveling distances above the continent are comparable for different air mass types, leading to similar δ_c values, which was what we actually measured.

Most of our measured δ_c values fell into the δ range of previous fog studies (from -71 ‰ to $+13$ ‰ for δ^2H and -10.4 ‰ to 2.7 ‰ for δ^{18}O in Scholl et al., 2007), except for a few, which were more depleted in ^{2}H and ^{18}O (Fig. 3). This is not surprising because most of the other measurements were performed at lower latitudes or in coastal areas where more enriched δ values are expected due to the nearby ocean source (Scholl et al., 2011). For a continental site, such as Schmücke, Rayleigh distillation by rain out is more pronounced than for a coastal measurement site.

The Cloud Water Line for our measurements CWL ($\delta_c^2\mathrm{H} = 7.8 \times \delta_c^{18}\mathrm{O} + 13.1 \times 10^{-3}$) was calculated by orthogonal regression, $R^2 = 0.96$. All our measured data lay above the GMWL. This was not expected a priori. First, other authors also found values below the GMWL (Scholl et al., 2011). Second, Local Meteoric Water Lines (LMWL) in central Europe have been found to be similar to the GMWL (Schoch-Fischer et al., 1983). This was also the case for the LMWL of the closest GNIP station, Wasserkuppe Rhön ($\mathrm{LMWL_{Wk}}$: $\delta_c^2\mathrm{H} = 8 \times \delta_c^{18}\mathrm{O} + 9.8 \times 10^{-3}$, 50°30′ N/9°57′ E, 921 m a.s.l.; 60 km west of the measurement station, see Fig. 1), which was deduced by orthogonal linear regression from δ values in precipitation from a data set collected between 1978 and 2007 based on monthly samples. It is probable that the lower deuterium excess of the precipitation ($\mathrm{LMWL_{Wk}}$) resulted

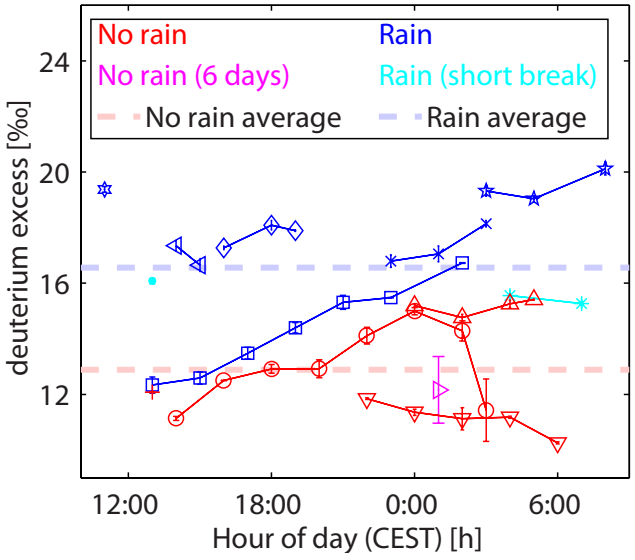

Fig. 4. Temporal evolution of the deuterium excess ($d = \delta^2H_c - 8 \times \delta^{18}O_c$) including measurement errors for the cloud events during HCCT-2010. Different symbols are used for the different events (see Table 1). Different colors are linked to precipitation at Schmücke. Red symbols are used if there was no rain since the last cloud event and pinc indicates that there was no rain within the last 6 days. The mean value of those values is indicated as a red dashed line. Blue is used for cloud events where precipitation did not stop one hour before the cloud event and cyan is used for cloud events when precipitation stopped within one day before the cloud event. The mean value of those cloud events is indicated as a blue dashed line.

from below-cloud evaporation of falling rain droplets. Decreases of the deuterium excess caused by below-cloud evaporation have been shown to be in the range of 1 to 4 ‰ for stations in Austria at a similar altitude during September and October, analyzing a 20-yr precipitation data set (precipitation-weighted monthly averages; Froehlich et al., 2008). Consequently, we assume that the difference between the precipitation $LMWL_{Wk}$ and the CWL at Schmücke are likely to result from below-cloud evaporation, which decreases the deuterium excess of the $LMWL_{Wk}$ with respect to the CWL.

3.1.2 Deuterium excess of the cloud water and moisture recycling

The deuterium excess ($d = \delta_c^2H - 8 \times \delta_c^{18}O$) of the Schmücke cloud samples was rather high (10 to 20 ‰, Fig. 4, mean value 14 ‰) as compared to European air moisture deuterium excess of 7 to 11 ‰ (Gat et al., 2003) and stayed rather constant during most of the cloud events, except for events 1 and 10, which are discussed in more detail in Sect. 3.2.3. Deuterium excess tended to be higher in cloud events that developed directly after rainfall (mean value: 17 ‰, blue dashed line in Fig. 4) than in cloud events that formed after a cloud free period without rainfall (mean value: 13 ‰, red dashed line in Fig. 4). The elevated deuterium excess could be an indicator of moisture recycling whereas a lower deuterium excess may represents an early stage condensation. However, as most cloud events were sampled during nighttime when evaporation rates are close to zero due to the lack of net radiative energy, moisture recycling due to evaporation of previously fallen precipitation was unlikely to happen directly at the site.

At this time of the year, precipitation at the site is commonly linked to large-scale precipitation occurring during frontal passages. This implies that precipitation at Schmücke is most likely occurring simultaneously with (or slightly delayed after) precipitation upwind of the measurement site. Consequently, the elevated deuterium excess of those cloud events sampled directly after rainfall was most probably caused by moisture recycling upwind of the Schmücke rather than by different climatic conditions at the initial moisture formation above the ocean. This view is in agreement with measurements of elevated deuterium excess presented by others both in rain and fog (Gat and Matsui, 1991; Rhodes et al., 2006; Froehlich et al., 2008; Cui et al., 2009).

3.2 Temporal evolution of δ values during different cloud events

In this section we focus on the temporal evolution of the δ_c values during each cloud event separately. The δ_c^2H and $\delta_c^{18}O$ values did not show any common trends in the evolution of the different cloud events. While the δ_c values decreased for events 3, 5 and 9 (✳, ◁, and ▽ in Fig. 3), they increased for events 1, 7 and 12 (□, ◇, and ☆) or first increased and then decreased (events 6 △, 10 ◯ and 11 ×).

However, looking at the data on a diurnal scale (Fig. 3) revealed highest δ_c values at night and lowest during daytime for at least six of the cloud events (Sect. 3.2.1). Furthermore, events 7 (◇) and 12 (☆) clearly differed from the other events with strongly increasing δ_c values with gradients of 0.6 ‰ per hour for $\delta_c^{18}O$ and 6 ‰ per hour for δ_c^2H (Sect. 3.2.2).

Independent of whether the cloud that we measured formed at the Schmücke or had already formed further away, the forced uplift of the air mass at Schmücke continuously fed the cloud with water vapor. As cloud droplets quickly achieve isotopic equilibrium with their surrounding vapor, we suggest two different reasons for the observed variations in δ_c values during the cloud events:

1. The observed variation results from changes in local temperature and condensed fraction, changing the δ values during condensation.

2. The observed variation is a consequence of changes in the δ values in the water vapor feeding the cloud.

The possible explanation 1 will be addressed in the next section by using the box model presented in Sect. 2.4 with measured temperature and vapor fraction as variables, and

assuming constant δ values of the water vapor feeding the cloud.

3.2.1 The contribution of condensation fractionation

The modeled isotopic dew point composition of the vapor ($\delta_{v,dew}$, a result from model runs A; Sect. 2.4.1) showed a similar diel pattern as the δ_c values of the condensed phase (Fig. 5a and c). Moreover, modeled monthly averages of $\delta_{v,dew}$ values for September and October were slightly more negative than the δ values measured in the water vapor of an 8-yr data set (Fig. 5b and d), taken on a 1 to 2 day basis in Heidelberg, located 227 km upwind of the Schmücke site (Jacob and Sonntag, 1991, see Fig. 1). This could result from the higher altitude of the measurement site or the uncertainty of the modeled $\delta_{v,dew}$ values. However, the δ values and their seasonal pattern were similar enough to assume that our modeled $\delta_{v,dew}$ values are reasonable and can be used as an input for model runs B. More generally, these results suggest as well that the δ values of water vapor can be estimated from cloud water samples.

Based on model runs B, the criterion for local condensation during the observation interval (Sect. 2.4.3) was fulfilled for part of the measurement period of event 6 (filled red △ in Fig. 5a and c) and 9 (▽). We therefore consider the temporal evolution of the δ_c values of these events to be basically determined by the local condensation process. The criterion was also met for two cloud samples of event 1 (□) and event 10 (◯). So, the temporal evolution of the isotopic signal of these two events was most likely affected mainly by an advected signal of the water vapor, and only for a short time by the condensation process. Additional samples also met the local condensation criterion either for $\delta^{18}O$ or for $\delta^{2}H$ (red in Fig. 5a and c). As condensation is supposed to be reflected in both $\delta^{2}H$ and $\delta^{18}O$ values, these data points were not classified as condensation driven. However, we cannot rule out that there might be some condensation contribution to the latter events as well. For the rest of the events, model results suggest the temporal pattern in δ_c values to be caused by the temporal pattern in the δ values of water vapor feeding the cloud rather than by condensation processes.

Interestingly, the two "condensation" cloud events (6 and 9) differ from the others in terms of overflow dynamics of the Schmücke mountain ridge as derived from the Froude number F (Fig. 5e). Event 6 (△) was categorized as stagnant area (F=2.33), and event 9 (▽) was categorized as stagnant flow (F=1.75). Hence, there was either a poor or no overflow over Schmücke for both events. This means that the air mass feeding the cloud most likely did not flow up the hill but it rather reached the measurement site on the same height. Consequently, these air masses might have been more decoupled from local sources, leading to a rather constant isotopic composition of the water vapor feeding the cloud (considering this air mass to be well mixed). This suggests that stable water isotope ratio measurements in combination with a box model can potentially complement meteorological sounding launches and tracer measurements to better assess whether cloud events can be qualified for the interpretation of Lagrangian type aerosol-cloud interaction experiment, where

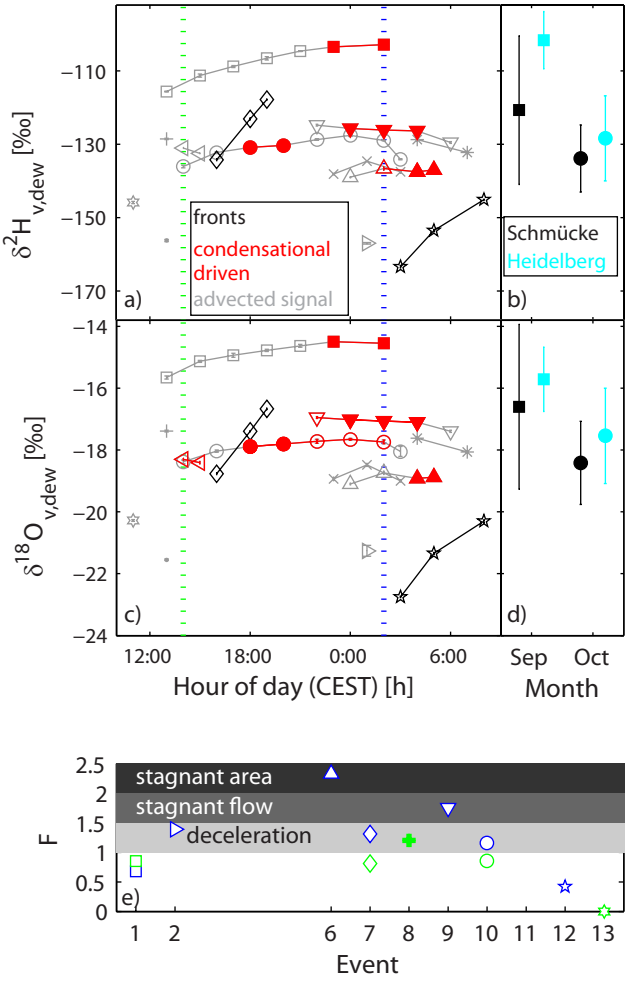

Fig. 5. δ values of the water vapor at dew point temperature calculated with model run A (Eq. 7) from the measured cloud water samples for $\delta^{2}H$ **(a)** and **(b)** and $\delta^{18}O$ **(c)** and **(d)**. Black symbols indicate high gradients in δ values in water vapor and liquid water samples, which could be associated to fronts. The measurements explainable by local condensational effects according to the criteria specified in Sect. 2.4 (using model run B) are plotted as filled red symbols. For open symbols, the condensational criteria were only met for either $\delta^{2}H$ or $\delta^{18}O$. The dotted blue and green vertical lines in panel **(a)** and **(c)** indicate the launch time of the meteo soundings in Meiningen (Fig. 1). **(e)** The Froude number F calculated from the profile data of these launches for the different events characterizes the overflow conditions at the measurement station, including the ranges of the overflow characterization as described in Sect. 2.3. Panels **(b)** and **(d)** show the monthly means and their variation for September and October for the equilibrium derived water vapor values at the dew point for Schmücke (black symbols) and for an 8 yr data set collected in Heidelberg (cyan symbols; Jacob and Sonntag, 1991).

good overflow conditions are essential. A good agreement of the box model output produced by model run A and B with the measured data then corresponds to a rather poor overflow, while a disagreement of the modeled and measured time course in δ_c^2H and δ_c^{18}O indicates a better overflow over the mountain ridge. We strongly recommend this to be further evaluated with future experiments.

3.2.2 Frontal passages

Events 7 (◇) and 12 (☆) were both characterized by a rather high mean deuterium excess (17.8 ± 0.4 ‰ for 7 and 19.5 ± 0.6 ‰ for 12, Fig. 4) and the highest gradients both in δ_c^2H (5.3 ‰ per hour for 7 and 4.0 ‰ per hour for 12) and in δ_c^{18}O (0.63 ‰ per hour for 7 and 0.49 ‰ per hour for 12; Fig. 3). Both events were associated with a frontal passage. In the case of event 7, a weak warm front passed during the cloud event, and a cold front preceded the cloud event 12 (Tilgner et al., 2012). No other measurements have been published yet resolving the isotopic composition of cloud water right after the passage of a cold front or during the passage of a warm front. In what follows we discuss how these results fit into the findings on front passages based on cumulative cloud samples and measurements of δ values of water vapor.

Similar observations of elevated deuterium excess during the passage of a cold front have been measured by Wen et al. (2008) in water vapor in Beijing. Water vapor originating from evaporation sites with low relative humidities may be the common feature explaining this similarity in deuterium excess observations during the passage of a cold front.

Cold fronts have been associated with more negative δ values in cumulative cloud samples (Scholl et al., 2007) as well as in water vapor (White and Gedzelman, 1984; Wen et al., 2008). This agrees with our data. The cold front carried ^{2}H- and ^{18}O-depleted water vapor causing the low δ_c values at the beginning of event 12. Continuous measurements of isotope ratios in water vapor also revealed that after the passage of a cold front, the δ values increased again (Lee et al., 2005). It is likely that we caught this increase of δ values with the clouds of event 12 (Fig. 3, ☆).

Warm sectors have been associated with more positive δ values of the water vapor (White and Gedzelman, 1984). We therefore expect an increase in δ_c values during the transition from the colder air in front of the warm front to the warm sector terminating the warm front. Based on the DWD synoptic charts (Sect. 2.3) the exact time of the frontal passage can not be determined, because the time resolution of the synoptic charts used in the framework of the HCCT-2010 analysis is 6 h exceeding the duration of cloud event 7.

However, the δ_c values indicate the warm front passage. The δ_c values of event 7 (Fig. 3, ◇) increased from the first cloud sample (which was similar to the ones from the previous cloud event (6, △) nine hours before) to the most positive δ_c values measured in October.

In summary, those cloud events associated with frontal passages were characterized by a strong increase in δ values and high deuterium excess, which is in agreement with what has been found for water vapor. However, further investigations of frontal passages are needed to compare the different changes in isotope ratios and effects of air mass origins, as frontal passages are linked to air mass changes and thus are important for air mass origin studies. In addition, understanding variability in isotope ratios is required to interpret monthly mean values of cloud water, which have been used for hydrological and ecological studies (Scholl et al., 2007).

3.2.3 Diel patterns: local water vapor sources versus moisture source region

The δ_c values of the cloud samples revealed a diel (nocturnal) pattern with highest values at night and lowest values during daytime (Fig. 3). This was especially pronounced in the two longest cloud events (1 and 10, both lasting 15 h) in δ_c^2H, δ_c^{18}O and deuterium excess. During event 1 (□) the δ_c values increased and during event 10 (◯) they first increased and then decreased. The peak-to-peak difference was 14 ‰, 1.2 ‰, and 4.4 ‰ for event 1 and 8 ‰, 0.5‰, and 3.8 ‰ for event 10 in δ_c^2H, δ_c^{18}O and deuterium excess, respectively.

Similar diel patterns – as well as peak to peak differences – have been measured for vapor phase δ values during dry conditions (below ≈ 80 % relative humidity) in populated areas (Lee et al., 2006; Wen et al., 2010), as well as above ecosystems (Lai et al., 2006; Welp et al., 2008). Different explanations have been given. Entrainment of ^{2}H- and ^{18}O-depleted vapor from the free atmosphere into the convective boundary layer at midday has been suggested (Wen et al., 2010). A combination of both atmospheric signal and biospheric signal (evapotranspiration) has been discussed as well (Lai et al., 2006; Welp et al., 2008).

Changes in isotopic composition of an air mass are either related to changes in temperature or rain out or by incorporation of new vapor through entrainment, transpiration or evaporation. Because the net radiative energy was either very small due to the cloudy environment (7 samples) or lacking (8 samples were collected at nighttime), we assume that the contributions of local evaporation and transpiration to the total moisture content of this air mass were small. Fog droplets equilibrate quickly with the advected vapor (Spiegel et al., 2012) and moreover, we could show that condensation only had a minor impact on the temporal evolution of these two events. Consequently, the temporal pattern in δ_c values that we measured in the cloud water was probably advected by the air mass. According to HYSPLIT ensemble trajectories analysis, the air mass feeding the cloud spent around 64 h (85 h) over land before reaching Schmücke, for event 1 and 10, respectively (van Pinxteren et al., 2011). So for both events, significant uptakes over land could have occurred, and we hypothesize the following processes that may

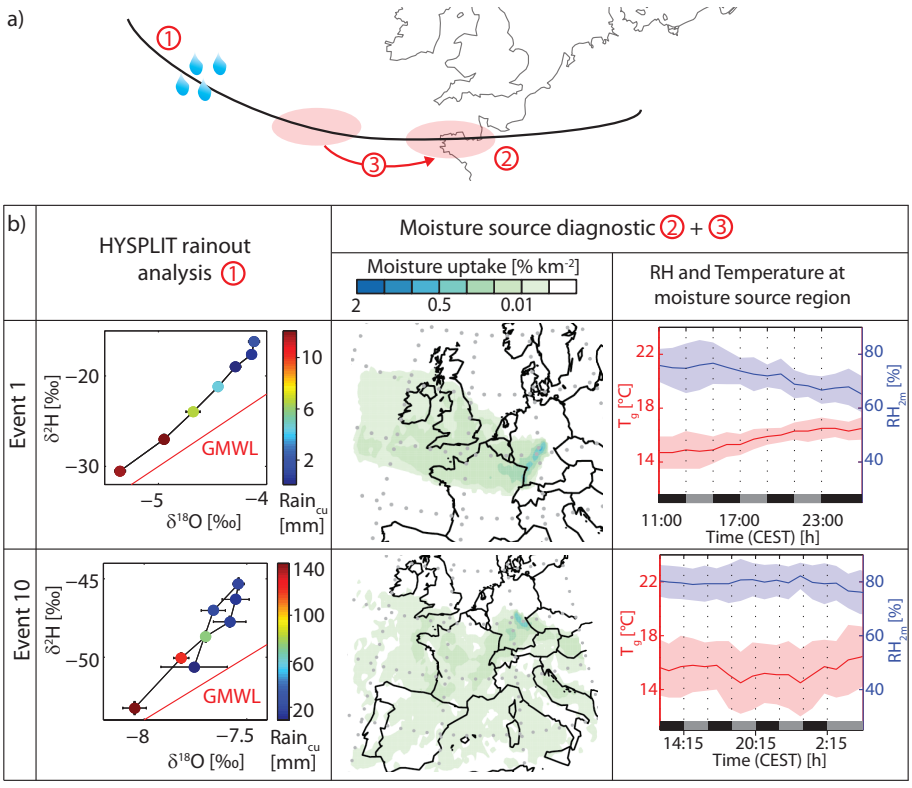

Fig. 6. Panel **(a)**: Suggested effects causing the δ_C variation during cloud events 1 and 10: ① rain out along the trajectory, ② meteorological changes in the source moisture region or ③ change of source moisture region. Panel **(b)**: Illustration of mechanism ①, ② and ③ for event 1 and 10. First column: cumulative rain along the HYSPLIT single trajectory for every measurement point as described in Sect. 2.3. Second column: geographical visualization of the moisture source region, deduced by the moisture source diagnostics (Sect. 2.3). Third column: temporal evolution of the relative humidity (blue) and temperature (red) at the moisture source region for the cloud sampling intervals indicated in black and gray.

have contributed to changes in isotopic composition of the fog droplets at Schmücke (Fig. 6):

1. The variations in the δ values of the advected and entrained vapor resulted from processes associated with air parcel history such as rain out.

2. Changes in relative humidity and temperature in the moisture source region (influencing transpiration and evaporation) caused changes in the δ values of the advected vapor.

3. The temporal evolution of the isotopic composition of these events was determined by geographical changes in moisture source region with distinct evaporative conditions (relative humidity, temperature or isotopic signature of soil water).

These processes were evaluated by a HYSPLIT rain out analysis (1) as well as by applying the moisture source diagnostic (2 and 3) as described in Sect. 2.3. Note that the rain out analysis has some degree of uncertainty as only a single trajectory was used. The rain out analysis showed strong rain out for the air parcels associated with the more depleted cloud water samples at the beginning of event 10 (Fig. 6b, column 1). A similar trend was observed for event 1, for which the rain out effect is smaller in amplitude. Hence, for both events, rain out prior to the arrival at Schmücke (1) would support the measured time trends.

The moisture source diagnostic revealed minor geographical changes in the moisture source region for both cloud events, so effect 3 can be ruled out. Event 1 is characterized by stable westerly to south westerly flow from the British Isles over northern France and south western Germany to Schmücke (Fig. 6b, column 2). During the cloud event, the relative humidity in the moisture source region decreased from 75 % to 65 %, while the temperature increased by 2°C (Fig. 6b, column 3). Event 10 is characterized by relative humidities above 80 % in the moisture source region until midnight, followed by a significant decrease in the early morning (Fig. 6b, column 3). The moisture source region for event 10 is large, indicating the importance of air mass mixing (Fig. 6b, column 3). However, the moisture sources contributing the most (darkest areas) are very closed to Schmücke, suggesting an important moisture contribution of regionally re-evaporated vapor.

The deuterium excess is a measure for kinetic isotope fractionation which is primarily influenced by the relative humidity at the evaporation site and generally not affected by rain out processes. Therefore it can be used as a proxy for the importance of remote effects changing the cloud water deuterium excess. Correlation between the relative humidity 2 m above the ground (RH_{2m}) with respect to ground temperature (T_g) at the moisture uptake location and the measured cloud water deuterium excess was found to be very high for event 1 (R^2=0.84) and very low (R^2<0.1) for event 10. Linear regression of the measured cloud water deuterium excess (d) with relative humidity at the source yields the following dependency for event 1:

$$d = -0.43\ ‰\ \%^{-1}\ \mathrm{RH}_{2\mathrm{m}}(T_g) + 46\ ‰ \quad (8)$$

This dependency of deuterium excess on the source relative humidity is close to the one found in earlier studies (Craig and Gordon, 1965; Merlivat and Jouzel, 1979; Pfahl and Wernli, 2008). Thus, the 4.4 % increase in deuterium excess as observed in the cloud water samples during the cloud event 1 could be explained by the decrease in moisture source relative humidity of 10 %. The higher relative humidities approaching saturation during event 10 are probably responsible for the weaker effect of kinetic isotope fractionation during evaporation. The strong mixing of different moisture sources increases the uncertainty in the identification method (consider the shaded area in Fig. 6b, column 3 representing the estimated moisture source condition), thus changes in the deuterium excess could not be related to changes in the moisture source relative humidity for event 10. Furthermore, due to the limited spectral resolution of the wind analysis data (7 km grid spacing) very localized recycling effects are likely underestimated by this method. Additional measurements of water vapor and cloud water during different meteorological conditions are needed to quantitatively assess the importance of the mechanisms of local transpiration, boundary layer dynamics and mixing of advected free atmospheric water vapor into the boundary layer.

4 Conclusions

We presented the first study resolving the temporal variation of δ^2H and δ^{18}O values of cloud droplets during single cloud events. The samples were taken during the HCCT-2010 campaign on Schmücke in central Germany. We focused on attempts to explain the temporal evolution of the isotopic signature on both event- and campaign scales. Our major conclusions are the following:

1. δ_c^2H and δ_c^{18}O values agreed with decreasing values towards winter as known from δ values in precipitation. Differences in deuterium excess were most probably related to continental moisture recycling.
2. Using a closed box model, we could identify two cloud events where the variation in δ_c values was mainly determined by changes in local temperature and vapor fraction during condensation, while for the rest of the cloud events, the variation in δ_c values was driven by the variation in δ values feeding the cloud. So cloud water samples could be used as a tool to assess questions of water vapor transport more precisely than by precipitation sampling, as cloud water is in isotope equilibrium with the surrounding vapor and as such is not biased by below-cloud evaporation. Moreover, there are hints that isotope ratios in cloud water could deliver information about the overflow characteristics over a mountain ridge during a cloud characterization experiment.
3. The temporal variations in δ values of cloud water were −3.6 to +1.7 ‰ per hour for δ_c^2H and −0.23 to +0.20 ‰ per hour for δ_c^{18}O, except for cloud events associated with frontal passages, where a steep increase in δ_c values was observed (>6 ‰ per hour for δ_c^2H and > 0.6 ‰ per hour for δ_c^{18}O). The temporal evolution of the isotopic composition during a frontal passage requires further measurements and research. It potentially provides interesting insights in air mass mixing effects and is an important input for air mass origin and budget studies.
4. Rain out and changes in relative humidity of the moisture source region most likely have contributed to the temporal trend that was observed in δ_c values and deuterium excess of the two overnight cloud events. We recommend parallel longterm measurements of δ values in cloud water at the site and water vapor at additional locations upwind of Schmücke (close by as well as further away like e.g. France, Italy and Scotland) for future measurement set ups to get a better understanding of the contribution of the advected δ values of the water vapor.

Acknowledgements. We thank Annika Ackermann for measuring the cloud water samples in the Isolab of the Grassland Sciences Group of ETH Zurich as well as Ansgar Kahmen for fruitful discussions. We thank the Swiss Meteorological Institute (MeteoSwiss) for providing the COSMO 7 km analysis data. Any use of trade, product, or firm names in this publication is for descriptive purposes only and does not imply endorsement by the US Government.

Edited by: M. C. Facchini

References

Araguas-Araguas, L., Danesi, P., Froehlich, K., and Rozanski, K.: Global monitoring of the isotopic composition of precipitation, J. Radioanal. Nucl. Chem., 205, 189–200, 1996.

Arends, B. G., Kos, G. P. A., Maser, R., Schell, D., Wobrock, W., Winkler, P., Ogren, J. A., Noone, K. J., Hallberg, A., Svenningsson, I. B., Wiedensohler, A., Hansson, H. C., Berner, A., Solly,

I., and Kruisz, C.: Microphysics of clouds at Kleiner Feldberg, J. Atmos. Chem., 19, 59–85, doi:10.1007/BF00696583, 1994.

Cappa, C. D., Hendricks, M. B., DePaolo, D. J., and Cohen, R. C.: Isotopic fractionation of water during evaporation, J. Geophys. Res., 108, 4525, doi:10.1029/2003JD003597, 2003.

Coplen, T.: Guidelines and recommended terms for expression of stable-isotope-ratio and gas-ratio measurement results, Rapid Commun. Mass Spectrom., 25, 2538–2560, doi:10.1002/rcm.5129, 2011.

Corbin, J. D., Thomsen, M. A., Dawson, T. E., and D'Antonio, C. M.: Summer water use by California coastal prairie grasses: fog, drought, and community composition, Oecologia, 145, 511–21, doi:10.1007/s00442-005-0152-y, 2005.

Craig, H.: Isotopic variations in meteoric waters, Science, 133, 1702, 1961.

Craig, H. and Gordon, L.: Deuterium and Oxygen-18 Variations in the Ocean and Marine Atmosphere, in: Stable Isotopes in Oceanic Studies and Paleotemperatures, edited by: Tongiorgi, E., 9–130, Consiglio Nazionale delle Richerche, Pisa, Italy, 1965.

Criss, R. E.: Principles of Stable Isotope Distribution, Oxford University Press, Oxford, 1999.

Cui, J., An, S., Wang, Z., Fang, C., Liu, Y., Yang, H., Xu, Z. and Liu, S. Using deuterium excess to determine the sources of high-altitude precipitation: Implications in hydrological relations between sub-alpine forests and alpine meadows, J. Hydrol., 373, 24–33, 2009.

Dansgaard, W.: Stable isotopes in precipitation, Tellus, 16, 436–468, 1964.

Dansgaard, W., Johnsen, S., Clausen, H., Dahl-Jensen, D., Gundestrup, N., Hammer, C., Hvidberg, C., Steffensen, J., Sveinbjörnsdottir, A., Jouzel, J., and Bond, G.: Evidence for general instability of past climate from a 250-kyr ice-core record, Nature, 364, 218–220, 1993.

Dawson, T. E.: Fog in the California redwood forest: ecosystem inputs and use by plants, Oecologia, 117, 476–485, doi:10.1007/s004420050683, 1998.

Demoz, B., Collett Jr., J. L., and Daube Jr., B.: On the Caltech active strand cloudwater collectors, Atmos. Res., 41, 47–62, doi:10.1016/0169-8095(95)00044-5, 1996.

Draxler, R.: Evaluation of an ensemble dispersion calculation, J. Appl. Meteor., 42, 308–317, 2003.

Draxler, R. and Hess, G.: Description of the HYSPLIT4 modeling system. NOAA Tech. Memo. ERL ARL-224, Tech. Rep. August 2002, Air Resources Laboratory Silver Spring, Maryland, USA, 1997.

Draxler, R. and Hess, G.: An overview of the HYSPLIT_4 modelling system for trajectories, dispersion, and deposition, Aust. Meteor. Mag., 47, 295–308, 1998.

Facy, L., Merlivat, L., Nief, G., and Roth, R.: The study of formation of hailstones by isotopic analysis, J. Geophys. Res., 68, 3841–3848, 1963.

Farquhar, G. D., Cernusak, L. A., and Barnes, B.: Heavy water fractionation during transpiration., Plant Physiol., 143, 11–18, doi:10.1104/pp.106.093278, 2007.

Feild, T. S. and Dawson, T. E.: Water sources used by *Didymopanax pittieri* at different life stages in a tropical cloud forest, Ecology, 79, 1448, doi:10.2307/176756, 1998.

Fischer, D. T. and Still, C. J.: Evaluating patterns of fog water deposition and isotopic composition on the California Channel Islands, Water Resour. Res., 43, W04420, doi:10.1029/2006WR005124, 2007.

Froehlich, K., Kralik, M., Papesch, W., Scheifinger, H., and Stichler, W.: Deuterium excess in precipitation of Alpine regions — moisture recycling, Isot. Environ. Health Stud., 44, 61–70, 2008.

Gat, J. R. and Matsui, E.:Atmospheric water balance in the Amazon Basin: An isotopic evapotranspiration model, J. Geophys. Res., 96, 13179–13188, 1991.

Gat, J. R.: Oxygen and hydrogen isotopes in the hydrologic cycle, Annu. Rev. Earth Planet. Sci., 24, 225–262, doi:10.1146/annurev.earth.24.1.225, 1996.

Gat, J. R.: Atmospheric water balance - the isotopic perspective, Hydrol. Process., 14, 1357–1369, doi:10.1002/1099-1085(20000615)14:8<1357::AID-HYP986>3.0.CO;2-7, 2000.

Gat, J. R., Klein, B., Kushnir, Y., Roether, W., Wernli, H., Yam, R., and Shemesh, A.: Isotope composition of air moisture over the Mediterranean Sea: an index of the air-sea interaction pattern, Tellus B, 55, 953–965, doi:10.1034/j.1600-0889.2003.00081.x, 2003.

Gedzelman, S.: Deuterium in water vapor above the atmospheric boundary layer, Tellus, 40B, 134–147, 1988.

Gehre, M., Geilmann, H., Richter, J., Werner, R., and Brand, W.: Continuous flow $^{2}H/^{1}H$ and $^{18}O/^{16}$ O analysis of water samples with dual inlet precision, Rapid Commun. Mass Spectrom., 18, 2650–2660, 2004.

Gerber, H.: Direct measurement of suspended particulate volume concentration and far-infrared extinction coefficient with a laser-diffraction instrument, Appl. Opt., 30, 4824–4831, 1991.

Heinold, B., Tilgner, A., Jaeschke, W., Haunold, W., Knoth, O., Wolke, R., and Herrmann, H.: Meteorological characterisation of the FEBUKO hill cap cloud experiments, Part II: Tracer experiments and flow characterisation with nested non-hydrostatic atmospheric models, Atmos. Environ., 39, 4195–4207, doi:10.1016/j.atmosenv.2005.02.036, 2005.

Henderson-Sellers, A., McGuffie, K. and Zhang, H. Stable isotopes as tools for global climate modle predictions of the impact of Amazonian deforestation, J. Clim., 15, 2664–2677, 2002.

Herrmann, H., Wolke, R., Müller, K., Brüggemann, E., Gnauk, T., Barzaghi, P., Mertes, S., Lehmann, K., Massling, A., and Birmili, W.: FEBUKO and MODMEP: Field measurements and modelling of aerosol and cloud multiphase processes, Atmos. Environ., 39, 4169–4183, doi:10.1016/j.atmosenv.2005.02.004, 2005.

Horita, J. and Wesolowski, D.: Liquid-vapor fractionation of oxygen and hydrogen isotopes of water from the freezing to the critical temperature, Geochim. Cosmochim. Acta, 58, 3425–3437, doi:10.1016/0016-7037(94)90096-5, 1994.

Hurni, L., editor: Atlas of Switzerland, Version 3, Swisstopo, Wabern-Bern, www.atlasofswitzerland.ch, 2010.

IAEA: Reference Sheet for VSMOW2 and SLAP2 international measurement standards. Issued 2009-02-13, International Atomic Energy Agency, Vienna, 5 pp., http://curem.iaea.org/catalogue/SI/pdf/VSMOW2_SLAP2.pdf, 2009.

Ingraham, N. L. and Mark, A. F.: Isotopic assessment of the hydrologic importance of fog deposition on tall snow tussock grass on southern New Zealand uplands, Austral Ecology, 25, 402–408, doi:10.1046/j.1442-9993.2000.01052.x, 2000.

Ingraham, N. L. and Matthews, R. A.: Fog drip as a source of groundwater recharge in northern Kenya, Water Resour. Res., 24, 1406, doi:10.1029/WR024i008p01406, 1988.

Jacob, H. and Sonntag, C.: A 8-year record of the seasonal variation of ^{2}H and ^{18}O in atmospheric water vapour and precipitation at Heidelberg, Germany, Tellus B, 43, 291–300, 1991.

Jouzel, J.: Teneur isotopique de la vapeur d'eau atmosphérique. Mise au point d'un système embarquable, J. Rech. Atmos., 13, 261–269, 1979.

Jouzel, J.: Isotopes in Clouds Physics: Multiphase and Multistage Condensation Processes, in: Handbook of Environmental Isotope Geochemistry, Volume 2, The Terrestrial Environment, B, edited by: Fritz, P. and Fontes, J., chap. 2, pp. 61–112, Elsevier Science Publischer B.V, Amsterdam, The Netherlands, 1986.

Jouzel, J., Masson-Delmotte, V., Cattani, O., Dreyfus, G., Falourd, S., Hoffmann, G., Minster, B., Nouet, J., Barnola, J. M., Chappellaz, J., Fischer, H., Gallet, J. C., Johnsen, S., Leuenberger, M., Loulergue, L., Luethi, D., Oerter, H., Parrenin, F., Raisbeck, G., Raynaud, D., Schilt, A., Schwander, J., Selmo, E., Souchez, R., Spahni, R., Stauffer, B., Steffensen, J. P., Stenni, B., Stocker, T. F., Tison, J. L., Werner, M., and Wolff, E. W.: Orbital and millennial Antarctic climate variability over the past 800,000 years, Science, 317, 793–6, doi:10.1126/science.1141038, 2007.

Knight, C. A., Knight, N., and Kime, K.: Deuterium content of storm inflow and hailstone growth layers, J. Atmos. Sci., 38, 2485–2499, 1981.

Lai, C.-T., Ehleringer, J. R., Bond, B. J., and Paw U, K. T.: Contributions of evaporation, isotopic non-steady state transpiration and atmospheric mixing on the δ^{18}O of water vapour in Pacific Northwest coniferous forests, Plant Cell Environ., 29, 77–94, 2006.

Lee, X., Sargent, S., Smith, R., and Tanner, B.: In situ measurement of the water vapor^{18}O/ ^{16}O isotope ratio for atmospheric and ecological applications, J. Atmos. Oceanic Technol., 22, 555–565, doi:10.1175/JTECH1719.1, 2005.

Lee, X., Smith, R., and Williams, J.: Water vapour ^{18}O/^{16}O isotope ratio in surface air in New England, USA, Tellus B, 58, 293–304, doi:10.1111/j.1600-0889.2006.00191.x, 2006.

Majoube, M.: Fractionnement en oxygène-18 et en deuterium entre l'eau et sa vapeur, J. Chim. Phys., 68, 1423–1436, 1971.

Merlivat, L. and Jouzel, J.: Global climatic interpretation of the deuterium-oxygen 18 relationship for precipitation, J. Geophys. Res., 84, 5029–5033, 1979.

Michna, P., Schenk, J., Wanner, H., and Eugster, W.: MiniCASCC – A battery driven fog collector for ecological applications, in: Proceedings of the Fourth International Conference on Fog, Fog Collection and Dew, La Serena, Chile, 22–27 July 200, July, 169–172, 2007.

Petit, J., Jouzel, J., Raynaud, D., Barkov, N., Barnola, J., Basile, I., Bender, M., Chappellaz, J., Davis, M., Delaygue, G., Delmotte, M., Kotlyakov, V., Legrand, M., Lipenkov, V., Lorius, C., Pepin, L., Ritz, C., Saltzman, E., and Stievenard, M.: Climate and atmospheric history of the past 420,000 years from the Vostok ice core, Antarctica, Nature, 399, 429–436, 1999.

Pfahl, S. and Wernli, H.: Air parcel trajectory analysis of stable isotopes in water vapor in the eastern Mediterranean, J. Geophys. Res., 113, D20104, doi:10.1029/2008JD009839, 2008.

Pierrehumbert, R. and Wyman, B.: Upstream Effects of Mesoscale Mountains, J. Atmos. Sci., 42, 977–1003, 1985.

Rank, D. and Papesch, W.: Isotopic composition of precipitation in the Mediterranean basin in relation to air circulation patterns and climate, in: IAEA-Tecdoc-1453, 19–35, Isotope Hydrology Section International Atomic Energy Agency, Vienna, Austria, 2005.

Risi, C.: Les isotopes stables de l'eau: applications à l'étude du cycle de l 'eau et des variations du climat, Phd, Université Paris, 2009.

Rhodes, A. L., Guswa, A. J. and Newell, S. E. Seasonal variation in the stable isotopic composition of precipitation in the tropical montane forests of Monteverde, Costa Rica, Water Resour. Res., 42, W11402, doi:10.1029/2005WR004535, 2006.

Rozanski, K., Araguas-Araguas, L., and Gonfiantini, R.: Isotopic Patterns in Modern Global Precipitation, in: Climate Change in Continental Isotope Records, edited by: Swart, P. K. and Lohman, K. C., vol. 78 of Geophysical Mongraph, 1–36, American Geophysical Union, 1993.

Scherhag, R.: Neue Methoden der Wetteranalyse und Wetterprognose, Springer, Berlin, 1948.

Schmid, S., Burkard, R., Frumau, K., Tobon, C., Bruijnzeel, L., Siegwolf, R., and Eugster, W.: Using eddy covariance and stable isotope mass balance techniques to estimate fog water contributions to a Costa Rican cloud forest during the dry season, Hydrol. Process., 25, 429–437, doi:10.1002/hyp.7739, 2010a.

Schmid, S., Burkard, R., Frumau, K., Tobon, C., Bruijnzeel, L., Siegwolf, R., and Eugster, W.: The Wet-canopy Water Balance of a Costa Rican Cloud Forest During the dry Season, in: Tropical Montane Cloud Forests, edited by: Bruijnzeel, L., Scatena, F., and Hamilton, L., p. 741, Cambridge University Press, Cambridge, 2010b.

Schoch-Fischer, H., Rozanski, K., Jacob, H., Sonntag, C., Jouzel, J., Östlun, G., and Geyh, M.: Hydrometeorological factors controlling the time variation of D, ^{18}O and ^{3}H in atmospheric water vapour and precipitation in the northern westwind belt, in: Isotope Hydrology, edited by: Street-Perrott, A., 3–30, IAEA Publications (SM-270/19), 1983.

Scholl, M., Eugster, W., and Burkard, R.: Understanding the role of fog in forest hydrology: stable isotopes as tools for determining input and partitioning of cloud water in montane forests, Hydrol. Process., 25, 353–366, doi:10.1002/hyp.7762, 2011.

Scholl, M. A., Giambelluca, T. W., Gingerich, S. B., Nullet, M. A., and Loope, L. L.: Cloud water in windward and leeward mountain forests: The stable isotope signature of orographic cloud water, Water Resour. Res., 43, 1–13, doi:10.1029/2007WR006011, 2007.

Sodemann, H., Schwierz, C., and Wernli, H.: Interannual variability of Greenland winter precipitation sources: Lagrangian moisture diagnostic and North Atlantic Oscillation influence, J. Geophys. Res., 113, D03 107, doi:10.1029/2007JD008503, 2008.

Spiegel, J. K., Aemisegger, F., Scholl, M., Wienhold, F. G., Collett Jr., J. L., Lee, T., van Pinxteren, D., Tilgner, A., Mertes, S., Herrmann, H., Werner, R. A., Buchmann, N., and Eugster, W.: Stable water isotopologue ratios in fog and cloud droplets of liquid clouds are not size-dependent, Atmos. Chem. Phys., 12, 9855–9863, doi:10.5194/acp-12-9855-2012, 2012.

Steppeler, J., Doms, G., Schättler, U., Bitzer, H. W., Gassmann, A., Damrath, U., and Gregoric, G.: Meso-gamma scale forecasts using the nonhydrostatic model LM, Meteor. Atmos. Phys., 82, 75–96, doi:10.1007/s00703-001-0592-9, 2003.

Tilgner, A., Bräuer, P., Schöne, L., Birmili, W., Mertes, S., van Pinxteren, D., and Herrmann, H.: Critical assessment of meteorological conditions and flow connectivity during HCCT-2010,

in preparation, 2012.

van Pinxteren, D., Brüggemann, E., Gnauk, T., Müller, K., Thiel, C., and Herrmann, H.: A GIS based approach to back trajectory analysis for the source apportionment of aerosol constituents and its first application, J. Atmos. Chem., 67, 1–28, doi:10.1007/s10874-011-9199-9, 2011.

Vimeux, F., Masson, V., Delaygue, G., Jouzel, J., Petit, J., and Stievenard, M.: A 420,000 year deuterium excess record from East Antarctica: information on past changes in the origin of precipitation at Vostok, J. Geophys. Res., 106, 31863, doi:10.1029/2001JD900076, 2001.

Welp, L. R., Lee, X., Kim, K., Griffis, T. J., Billmark, K. A., and Baker, J. M.: δ^{18}O of water vapour, evapotranspiration and the sites of leaf water evaporation in a soybean canopy, Plant Cell Environ., 31, 1214–1228, doi:10.1111/j.1365-3040.2008.01826.x, 2008.

Wen, X., Sun, X., Zhang, S., Yu, G., Sargent, S., and Lee, X.: Continuous measurement of water vapor D/H and ^{18}O/^{16}O isotope ratios in the atmosphere, J. Hydrol., 349, 489–500, doi:10.1016/j.jhydrol.2007.11.021, 2008.

Wen, X.-F., Zhang, S.-C., Sun, X.-M., Yu, G.-R., and Lee, X.: Water vapor and precipitation isotope ratios in Beijing, China, J. Geophys. Res., 115, D01103, doi:10.1029/2009JD012408, 2010.

Wernli, H. and Davies, H. C.: A Lagrangian-based analysis of extratropical cyclones. I: The method and some applications, Quart. J. Roy. Meteor. Soc., 123, 467–489, doi:10.1002/qj.49712353811, 1997.

White, J. and Gedzelman, S.: The isotopic composition of atmospheric water vapor and the concurrent meteorological conditions, J. Geophys. Res., 89, 4937–4939, 1984.

Yakir, D. and Sternberg, L. d. S. L.: The use of stable isotopes to study ecosystem gas exchange, Oecologia, 123, 297–311, doi:10.1007/s004420051016, 2000.